Novel D–A chromophores with condensed 1,2,4-triazine system simultaneously display thermally activated delayed fluorescence and crystallization-induced phosphorescence

Antonio Maggiore, Xiaofeng Tan, Arnaud Brosseau, Andrew Danos, Fabien Miomandre, Andrew Monkman, Pierre Audebert, Gilles Clavier

Novel D–A chromophores with condensed 1,2,4-triazine system simultaneously display thermally activated delayed fluorescence and crystallization-induced phosphorescence†

Antonio Maggiore*[ab], Xiaofeng Tan[c], Arnaud Brosseau[a], Andrew Danos[d], Fabien Miomandre[a], Andrew P. Monkman[d], Pierre Audebert[a], Gilles Clavier[a]

[a] Université Paris-Saclay, ENS Paris-Saclay, CNRS, PPSM, 91190 Gif-sur-Yvette, France.
[b] CNR-NANOTEC – Institute of Nanotechnology, c/o Campus Ecoteckne, Via Monteroni, 73100 Lecce, Italy
[c] Department of Polymer Chemistry and Technology, Kaunas University of Technology, Radvilenu plentas 19, LT50254 Kaunas, Lithuania
[d] Physics Department, Durham University, Durham DH1 3LE, UK

† Electronic supplementary information (ESI) available. See DOI: https://doi.org/10.1039/d2cp00777k

Phys. Chem. Chem. Phys., 2022, 24, 17770-17781 DOI: 10.1039/D2CP00777K

Received 15th February 2022 , Accepted 21st June 2022 First published on 4th July 2022

Abstract

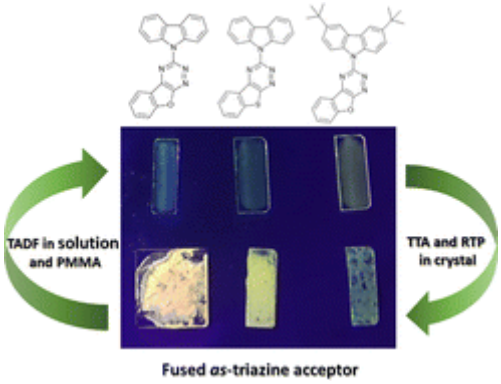

Control of photophysical properties is crucial for the continued development of electroluminescent devices and luminescent materials. Preparation and study of original molecules uncovers design rules towards efficient materials and devices. Here we have prepared 7 new compounds based on the popular donor–acceptor design used in thermally activated delayed fluorescence emitters. We introduce for the first time benzofuro[3,2-*e*]-1,2,4-triazine and benzothieno[3,2-*e*]-1,2,4-triazine acceptors which were connected to several common donors: phenoxazine, phenothiazine, carbazole and 3,6-di-tert-butylcarbazole. DFT calculations, and steady-state and time-resolved photophysical studies were conducted in solution and in solid states. While derivatives with azine moieties are non-emissive in any form, the compounds comprising 3,6-di-tert-butylcarbazole display TADF in all cases. More interestingly, the two derivatives substituted with a carbazole donor are TADF active when dispersed in a polymer matrix and phosphorescent at room temperature in neat films (microcrystalline form).

Introduction

Efficient luminescent organic materials are in high demand for the development of optoelectrical devices and sensors. Control of the photophysical properties and emission nature is of crucial importance for these applications. For example, Thermally Activated Delayed Fluorescence (TADF) has gained high popularity for electroluminescent (EL) devices after the pioneering work of Adachi,[1–5] because it enables high efficiency by harvesting both singlet and triplet states to produce light (while avoiding the use of expensive metals). On the other hand, Room Temperature Phosphorescence (RTP) is very attractive in bioimaging because it allows easy implementation of time-gated imaging (avoiding autofluorescence interferences) while large Stoke shifts eliminate the necessity to use expensive filters to remove excitation light.[6,7]

The TADF phenomena can occur when a small singlet–triplet energy splitting (ΔE_{ST}) is obtained through, *e.g.* a charge transfer (CT) transition using donor–acceptor (D–A) compounds.[8–10] Indeed, in D–A compounds the highest occupied molecular orbital (HOMO) and the lowest unoccupied molecular orbital (LUMO) are separated on different moieties of the molecule minimizing exchange energy and thus also ΔE_{ST}. This leads to efficient reverse intersystem crossing (r_{ISC}) from T_1 to S_1. Many reports now exist of efficient TADF emission achieved through a pre-twisted charge transfer configuration in D–A–D systems with a certain degree of HOMO–LUMO overlap.[11–20] Consequently, a proper choice of D and A moieties as well as their linkage pattern are very important parameters to obtain efficient TADF emitters.[8,21–23] Recently, an alternative approach to achieve small ΔE_{ST} has appeared, consisting in the use of p- and n-doped polycyclic aromatic hydrocarbons. This leads to so-called multi-resonance TADF (MR-TADF) materials[24–28] which present interesting and useful properties in terms of colour purity and narrowed emission bandwidth, revealing that not only intersegmental but also interatomic D–A interactions can be used to achieve TADF.

On the other hand, RTP has been observed when molecules with larger ΔE_{ST} are in an environment where molecular motions are restricted.[29] In particular, reliable methods to induce efficient RTP include aggregation or crystallization-induced enhanced emission (AIEE or CIEE).[30] Crystallization-induced RTP results from the formation of highly ordered crystalline structures, which restricted molecular motion inside the crystal lattice (suppressing vibrational modes coupled to non-radiative decay pathways) and also prevent oxygen diffusion and direct quenching of the triplet excited states and their phosphorescence. Switching between the two delayed emission properties can thus be sometimes observed with only minor environmental or chemical changes.

Among all the acceptors used in TADF, triazines have attracted great attention because of their strong electron deficiency and ability to undergo various functionalizations.[31–36] There are two possible triazine isomers: symmetric 1,3,5-triazine (*s*-triazine), and asymmetric 1,2,4-triazine (*as*-triazine).[33] A third possible isomer, 1,2,3-triazine, is stable only when incorporated in fused ring systems and so has not received similar attention. *s*-Triazine has received the greatest interest, because of the availability of numerous and cheap synthetic feedstocks and reaction schemes. It has been widely used to synthesize excellent electron transporting materials, host materials, emitters, and ligands for organometallic phosphorescent complexes used in OLEDs.[37,38] Consequently, numerous publications deal with 1,3,5-triazines based luminescent TADF materials.[39,40] In particular, Adachi *et al.* prepared a green TADF OLED with a maximum EQE of 29.6% using a *s*-triazine based emitter.[41]

The asymmetric *as*-triazine unit has only rarely been used as a building block for organic active materials, especially as an OLED emissive layer.[33,41] Recently Xiang *et al.*[42] reported TADF emitters featuring an *as*-triazine core as the electron acceptor and 2 or 3 phenoxazines as donors. The tris-phenoxazinyl-*as*-triazine based OLED displayed yellow emission and achieved a good EQE of 13.0%, which is comparable to similar devices based on *s*-triazine. Xiang's work demonstrated the potential of *as*-triazine as a building block towards efficient luminescent materials. *as*-Triazine can also be condensed with other aromatic rings to form new extended aromatic structures.[43] Investigations of such fused 1,2,4-triazine systems as luminescent materials has not been reported, until now.

In this work we prepared and studied new fused 1,2,4-triazines: benzofuro[3,2-*e*]-1,2,4-triazine and benzothieno[3,2-*e*]-1,2,4-triazine, each substituted with various common donors (carbazole, phenoxazine, phenothiazine and 3,6-di-*tert*-butylcarbazole, Fig. 1). Interestingly, we show that if their molecular motion is restricted, it is possible to switch the emission of two of these derivatives from TADF to RTP by changing their aggregation state. Indeed, these derivatives show TADF when dispersed in a PMMA matrix at RT, but RTP in neat films (microcrystalline form).

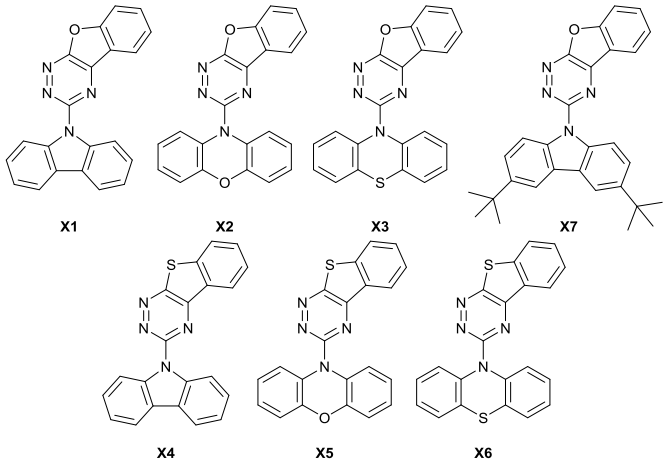

Fig. 1 Molecular structures of the new fused 1,2,4-triazines synthesized and studied in this work

Results and discussion

Synthesis and theoretical chemistry

Synthesis The first steps of the synthetic pathway were inspired by the work of Seitz et al.[44] The benzofuro[3,2-*e*]-1,2,4-triazine and benzothieno[3,2-*e*]-1,2,4-triazine were prepared starting from the 3,6-dichloro-*s*-tetrazine in two steps: (a) a nucleophilic aromatic substitution (S_NAr) followed by (b) an intramolecular cycloaddition (Scheme 1). The intermediates produced by this sequence still bear a chlorine atom that can undergo a second S_NAr reaction with heterocyclic donors to yield the final adducts (Scheme 1).

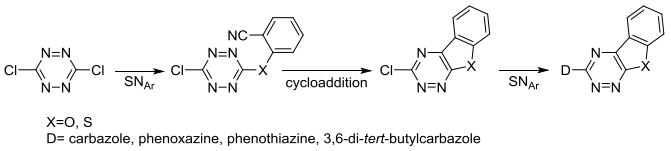

Scheme 1 Synthetic pathway used to prepare the new donor substituted benzofuro[3,2-*e*]-1,2,4-triazines and benzothieno[3,2-*e*]-1,2,4-triazines.

All compounds have been characterized by ^1H and ^{13}C NMR and mass spectrometry (see ESI†). Their thermal stabilities have also been evaluated by thermal gravimetric analysis (TGA). The compounds show good stability with a thermal decomposition temperature (Td, corresponding to 5% weight loss) ranging from 285 to 320 °C (Table S1, ESI†).

DFT calculations All compounds have been studied by DFT calculation (see ESI† for details) to facilitate interpretation of subsequent experimental photophysical data. First, the ground state geometries of the derivatives were obtained (Fig. 2 and Fig. S1, ESI†). The calculated structures of the benzofuro[3,2-*e*]-1,2,4-triazines and benzothieno[3,2-*e*]-1,2,4-triazines acceptors are flat in all cases (angle A in Table S2, ESI†). In the case of **X1**, **X4** and **X7** the carbazole donor is flat (Fig. 2 and angle D in Table S2, ESI†) and the D and A subunits are almost fully conjugated (Fig. 2 and angle A–D <20° in Table S2, ESI†). This is consistent with a recent report showing that in spatially compact pyrazine acceptor heteroatoms allow TADF donors to twist more freely than when surrounded by C–H bonds or other donors.[45] However, when D is a bulkier phenoxazine (**X2** and **X5**) or a phenothiazine (**X3** and **X6**) the donor is tilted (angle 35 or 47°, Fig. S1 and angle D in Table S2, ESI†) and D and A are quasi axial (angle A–D in Table S2, ESI†) as previously noticed for similar compounds.[46]

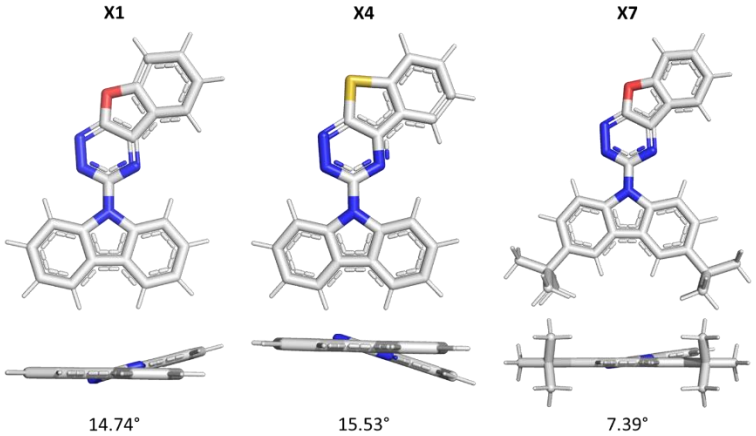

Fig. 2 Optimized ground state structures of **X1** (left), **X4** (center) and **X7** (right). The number below the structures refers to the D–A angle which is the calculated angle between the mean planes of the donor and the acceptor.

The calculated energies of the frontier molecular orbitals show that the benzofuro[3,2-*e*]-1,2,4-triazine has a slightly stronger acceptor character than the benzothieno[3,2-*e*]-1,2,4-triazine with the LUMO of the former approximately 0.08 eV lower in energy (Fig. S2, ESI†). In all cases, the HOMO is delocalized on the donor moiety with a small participation from the *as*-triazine, while the LUMO is localized exclusively on the acceptor moiety (Fig. S3 top, ESI†).

TDDFT calculations reveal that the lowest energy singlet transition corresponds to a D–A charge transfer (CT) state, while the second lowest is an *as*-triazine centred n–π* transition (Fig. S3 bottom and Table S3, ESI†). Higher energy transitions have a π–π* character and are centred on either the D or A moieties (locally excited, LE). Table S4 (ESI†) is reports the D index which is a magnitude of CT length and t index which is designed to measure the degree of separation of hole and electron for the first transition. Both indices are large for all compounds thus indicating the CT nature of the first calculated transition. It is also confirmed visually with the plots of the charge density differences between excited state and ground state (Fig. S4, ESI†). The calculated wavelength values for the first transition are in good agreement with the experimental ones (Table S6, ESI,† mean averaged error less or equal to 10%).

The geometries of the first singlet excited state (S_1) of each compound were then optimised (Fig. S5, ESI†). For **X1**, **X4** and **X7**, the D–A angle increases from less than 20° in the S_0 state to ≈52° in the S_1 state (Table S5, ESI†). The MOs also become less delocalized so the S_1 state has a more pronounced CT character than the first excited state at S_0 geometry as indicated by the increase of the magnitude of both D and t indexes (Table S4, ESI†) and ΔE_{ST} is ≈ 0.1 eV. For the other derivatives, D becomes flat and the D–A angle is close to 90° (quasi-equatorial configuration).[46] D and A are orthogonal and S_1 is a pure CT state with strong stabilization and very small ΔE_{ST} (0.02 eV).

In conclusion, when D is a phenoxazine or a phenothiazine, the compounds should be non-emissive because the pure CT character leads to a symmetry-forbidden transition. When D is instead a carbazole moiety, the derivatives should possess mixed-character excited states more suited for prompt and delayed fluorescence.

Photophysical study

The compounds substituted by phenothiazine or phenoxazine moieties (**X2**, **X3**, **X5** and **X6**), display less remarkable emissive properties than the ones substituted by a carbazole moiety (**X1**, **X4** and **X7**). Indeed, as predicted by our computational study, **X2**, **X3**, **X5** and **X6** are almost totally non-emissive

(Table S7, ESI†) with measurable emission quantum yields (QY) in only limited cases (Table S8, ESI†). Therefore, a detailed photophysical study has only been carried out on the emissive compounds featuring carbazole donors: **X1**, **X4** and **X7**.

*Photophysical study of the azine-donor compounds (**X2, X3, X5** and **X6**)* UV-Vis absorption spectra of **X2**, **X3**, **X5** and **X6** are reported in Fig. S6 (ESI†). At low energy, absorption spectra exhibit two weak bands in the 350–500 nm region (Table S7, ESI†). Based on the TDDFT results, the lower energy one is assigned to a CT transition derived from electron transfer from the HOMO of the donor (phenoxazine) to the LUMO of the acceptor (*as*-triazine). The second band is a n–π* transition located on the triazine core, as noticed before in simple triazines.[47,48] At a higher energy, **X2** and **X5** exhibit two absorption bands with λ_{max} *ca.* 280 nm and 310 nm, which are typical of phenoxazine derivatives.[49,50] **X3** and **X6** compounds also present an intense band with a shoulder in that range that is typical of phenoxazine derivatives.[49,50]

The steady state emission spectra of **X2**, **X3**, **X5** and **X6** in solution (cyclohexane and toluene) and in solid state (PMMA, neat film, and crystal powder) are shown in Fig. S7 (ESI†). The neat films for these four compounds appear amorphous and glassy. All the molecules can be considered as quasi-non-emissive in solution even if a very weak emission (around 395 nm typical of the phenoxazine[49]) is detectable for **X2** and **X5** in non-polar solvents *i.e.* cyclohexane and toluene. This non-emissive categorization is supported by very low measured QYs, in many cases near zero (Table S8, ESI†).

When dispersed in PMMA (a rigid matrix at RT), all compounds display a CT emission although with very low intensity (Fig. S7, ESI†). At best, **X3** and **X6** present a measurable QY of 0.2% (Table S8, ESI†). In addition, the LE fluorescence band of phenoxazine is also present, especially for **X5**. Moreover, in Fig. S7 (ESI†) we can notice that **X2**, **X3** crystals and **X5** neat film maintain a CT emission band similar to the one in PMMA thus retain the fluorescence of a single molecule in the crystal or neat film (both in spectral shape and position). Interestingly the crystalline powder of **X2** and **X6** show a more intense emission (0.5%) than the molecule dispersed in PMMA. Therefore, we identify a moderate Crystallization Induced Enhanced Emission (CIEE) phenomenon in these materials. However, in **X6** crystal we observe a bathochromic shift respect to PMMA that indicates the formation of a different emissive excited state (e.g. dimer, excimer).

Fluorescence decays were recorded for the compounds dispersed in PMMA and we observed two emission decay lifetimes, in the nanosecond and microsecond regimes (Table S8, ESI†). It can thus be concluded that despite weak intensities both prompt and delayed fluorescence channels are present. A similar result was obtained for the most emissive **X2** and **X6** crystalline powders (Table S8, ESI†).

*Photophysical study of the carbazole-donor molecules (**X1, X4** and **X7**) in solution* The UV-Vis absorption spectra of molecules **X1**, **X4** and **X7** are displayed in Fig. 3. All molecules exhibit a twofold broad absorption band between 370 and 470 nm (Table S7, ESI†). Similar to the previous materials, the lower energy maximum is attributed to a CT state coming from an electron transfer from the HOMO of the donor (carbazole) to the LUMO of the acceptor (triazine), with the second band arising from a n–π* transition located on the triazine core.[48] The three higher energy absorption bands (Table S7, ESI†) are associated with π–π* transitions due to their larger relative intensity. These absorption bands peaking at λ_{max} = 325–330 nm and λ_{max} ≈ 292 nm are typical of carbazole derivatives.[51–53]

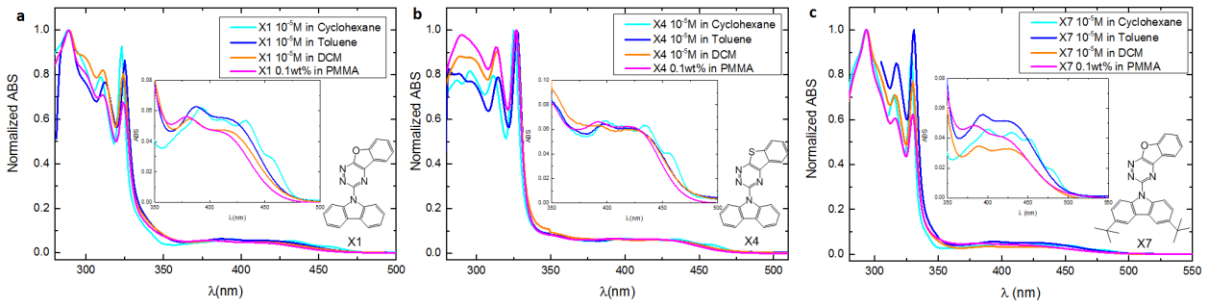

Fig. 3 Absorption spectra of **X1** (a), **X4** (b) and **X7** (c) in cyclohexane (10^{-5} M, cyan), toluene (10^{-5} M, blue), dichloromethane (10^{-5} M, orange) and PMMA (0.1wt%, pink). Inset in all four graphs: zoom of the low energy bands between 350 nm and 500 nm.

To investigate the effect of the different donor and acceptor moieties on the maximum emission wavelength, we compared the photoluminescence (PL) spectra of the compounds in toluene (Fig. 4). First we compared **X1** and **X7** which differ by the nature of their donor; carbazole and 3,6-di-*tert*-butylcarbazole respectively. The inductive effect is stronger with the latter, causing it to act as a stronger donor. The different steric hindrance is irrelevant in fluid solution because of the remote position of the substituents. The emission maxima (and colour) for **X1** and **X7** are 543 nm (green) and 598 nm (orange) respectively (Table S7, ESI†). This is in accordance with the stronger donor character of the 3,6-di-*tert*-butylcarbazole. We also compared **X1** and **X4**, which only differ by their acceptor units: benzofuro- and benzothieno-*as*-triazine respectively. The replacement of oxygen (**X1**) by sulphur (**X4**) in the acceptor unit weakly affects their emission maxima (Fig. 4) which shift by only 10 nm (**X4** = 533 nm). This change is in accordance with the DFT calculations, and shows that the benzofurotriazine is a slightly stronger acceptor than the benzothienotriazine. However, their QYs are strongly affected by this change, with **X1** twice as emissive as **X4** in aerated toluene (Table 1). This might be due to the "heavy atom effect" induced by the presence of sulphur (relative to the much lighter oxygen) which can promote intersystem crossing that competes with emission, leading to a lower QY.

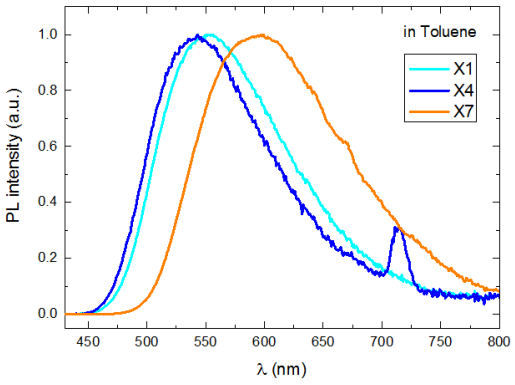

Fig. 4 Photoluminescence spectra of **X1** (cyan), **X4** (blue) and **X7** (orange) in toluene (10^{-5} M). λ_{ex}=325-327 nm

Table 1 Spectroscopic properties of **X1**, **X4** and **X7** in toluene.

	QY (air) (%)	QY (deg) (%)	FWHM (nm)	ΔE_{ST} (S1-T1) (eV)*	$\tau_{1,av}$ (ns)	$\tau_{2,av}$ (µs)
X1	0.98	1.40	127	0.47	3.10	4.70
X4	0.46	0.55	119	0.50	1.00	2.01
X7	1.00	1.60	146	0.43	3.15	11.08

We have also investigated the influence of solvent polarity on the fluorescence emission in solution of the three compounds, as the emission wavelength of a molecular system with a CT emitting state generally undergoes a large red-shift as the polarity of the solvent increases.[54,55] Fig. S8 (ESI†) displays the normalized PL spectra of **X1**, **X4** and **X7** in three different solvents. For all three molecules, the emission maximum indeed exhibits a strong red-shift as the polarity of the solvent increases (Fig. S8, Table S7, ESI†). The emission band of all three compounds in cyclohexane is well resolved and structured, atypical of CT states. This indicates that the S_1 state has a weak CT character in non-polar solvents, instead displaying features of localised excitons (LE character). This is due to cyclohexane's very small solvent dipole moment that cannot stabilize efficiently a CT state. The fluorescence in cyclohexane hence comes from a mixed LE and CT state. In the more polar toluene and dichloromethane, a typical broad CT emission is observed for all three compounds. In those solvents the interactions between the excited state dipole moment of the compounds and the dipole moment of the solvent are stronger, and they promote the stabilisation of the excited CT state.

TADF properties of **X1**, **X4** and **X7** were evaluated in solution by comparison of aerated and degassed cyclohexane and toluene emission QY (Table 1 and Table S10, ESI†). The low QYs of these three compounds are not affected by oxygen in cyclohexane indicating that the emission arises mostly from PF. In fact, the effect of O_2 quenching is particularly evident with long-lived emissive states. Nevertheless, a negligible TADF contribution can be also detected as demonstrated by the long-lived transient PL decay in deoxygenated solution (Fig. S10, ESI†). On the other hand, the QYs in toluene increase more than threefold compared to cyclohexane, and increase by a further 50% in absence of oxygen. Together with their broad emission band, this is consistent with the existence of the long-lived excited states (such as from TADF) in toluene for these compounds.

Analysis of the transient PL decay profiles of the three compounds in degassed toluene (Table 1 and Fig. S9, S10, ESI†) further establishes the occurrence of an up-conversion phenomenon. The transient decay profiles display two components; the first can be assigned to the prompt emission derived from the direct $S_1 \rightarrow S_0$ transition, which has an average lifetime (τ_1 in Table 1) of *ca.* 1–3 ns. The second one is much longer lived (in the µs range; τ_2 in Table 1) and is assigned to the delayed fluorescence resulting from the successive ISC and rISC up-conversion of the excitons from the T_1 state to the S_1 state, followed by fluorescence emission. We can notice that **X4** presents τ_1 and τ_2 much shorter than **X1** and **X7**, likely due to the sulphur atom inducing larger k_{nr}. A rough estimation using QY(air) and τ_1 shows that prompt k_r is similar in the three cases ($3–4 \times 10^6$ s^{-1}) while prompt k_{nr} is much larger for **X4** (9.9×10^8 s^{-1}) than for **X1** and **X7** ($3.1–3.2 \times 10^8$ s^{-1}). The typical effect of fluorescence quenching by heavier atoms (more vibronic states available) likely explains this difference.

*Photoluminescence of the carbazole-donor molecules (**X1**, **X4** and **X7**) in solid state (PMMA, neat film, crystal)* We also investigated the photophysical properties of **X1**, **X4** and **X7** in the solid state under three different forms (see preparation in ESI†):

- Molecules dispersed in PMMA films (0.1 wt%), to study the isolated molecules emission in a rigid matrix.

- Neat films prepared by drop-casting of DCM solutions on a quartz slide. The neat films for all three compounds were visually polycrystalline.

• As-synthesized polycrystalline powders studied in a 1 mm quartz cuvette.

Interestingly, the PL spectra of all three compounds are significantly different in the three different forms (Fig. 5). The emission in PMMA appears as a broad featureless band for all three compounds, indicating that it arises from a CT state. However, the emission in PMMA is blue-shifted compared to toluene (26 nm for **X1**, 21 nm for **X4**, and 55 nm for **X7**). This is due to a rigidochromic effect in PMMA, that limits rotational molecular motions and geometric stabilization of the CT excited state which can proceed unhindered in fluid solution.

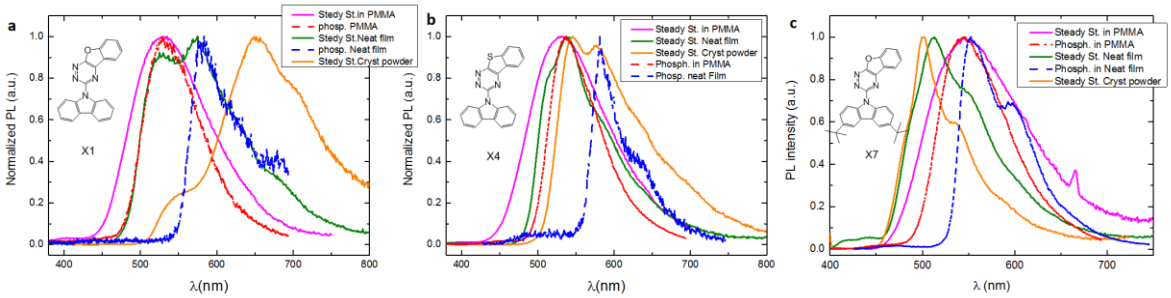

Fig. 5 Photoluminescence spectra (in air) of **X1** (a), **X4** (b) and **X7** (c) in PMMA (pink), in PMMA phosphorescence (red dashed), neat film (green), neat film phosphorescence (blue dashed) and polycrystalline powder (orange). λ_{exc} = between 325–330 nm.

The maximum emission wavelengths of the neat film microcrystalline samples of **X1** and **X4** are red-shifted with respect to the PMMA samples (Table 2), while conversely it is blue-shifted for **X7**. The observed difference must arise from the presence of the *tert*-butyl groups in **X7**. Indeed, those bulky substituents probably restrict close packing of the PMMA chains towards individual **X7** molecules in PMMA, providing spatial freedom for geometry relaxation in the excited state that leads to stabilisation of the twisted CT excited state and red-shifted emission in the polymer.

Table 2 Maximum emission wavelengths and band onset for **X1**, **X4** and **X7** in PMMA, neat film and powder (s denotes a shoulder instead of a maximum)

	PMMA		**neat film**		**powder**	
	λ_{max}(nm)	**E_{ons}(eV)**	**λ_{max}(nm)**	**E_{ons}(eV)**	**λ_{max}(nm)**	**E_{ons}(eV)**
X1	530	2.74	530, 575, 640s, 685s	2.57	545,650, 705s	2.43, 2.35
X4	532	2.72	518s,538, 575s, 639s	2.56	546,576, 640,700s	2.46
X7	545	2.64	512,545s,590s	2.67	500,535,583s	2.70

s =shoulder

In powders and neat films, **X1** and **X4** show clearly different spectra from PMMA (Fig. 5a and b). Multiple bands are present and the emission onset is red-shifted when moving from PMMA to the neat crystal and to the crystalline powder. This effect is particularly marked for **X1**, where the emission maximum of the crystalline powder is shifted more than 150 nm with respect to PMMA. The powder and neat film of **X7** (Fig. 5c) display narrower, blue-shifted bands compared to PMMA. However, as the onset of the bands lies close in energy, the emission in the three forms most likely originates from the same excited state. The freer geometry relaxation in S_1 for **X7** in PMMA results in its more Gaussian and redshifted emission in this host. The differences observed in **X7** may also be

related to the ability of the tert-butyl groups to disrupt aggregates (e.g. dimers, excimers) that otherwise form in **X1** and **X4** through π–π interactions.[56–58] Those aggregates possess a very different photophysical behaviour from the isolated single molecules.[59] The *tert*-butyl groups in **X7** also maintain molecular separation in the crystalline solids, and so **X7** always retains properties closer to isolated molecules.

Time-resolved photophysical properties in PMMA Photophysical properties of **X1**, **X4** and **X7** dispersed in a PMMA matrix (0.1 wt%) were further studied by time-resolved emission spectroscopy to gain insight into the nature of the states involved in the prompt and delayed emission. All measurements were performed using an iCCD camera and spectrograph, with individual spectra captured at specific time delays (TD), with given integration times (IT) after pulsed laser excitation. This technique enables simultaneous construction of decay curves with associated spectral data by collecting several spectra with logarithmically increasing TD and IT.[60] The data were collected under vacuum at RT and under a stream of nitrogen at 77 K.

Two main material properties were typically encountered. When the emission spectra remain constant throughout the decay, this means that the luminescence arises from the same singlet state throughout. The observed delayed emission is due to the population of the triplet state, that up-converts back to the singlet through rISC (TADF) or possibly by triplet–triplet annihilation (TTA). We suggest that bi-excitonic TTA is extremely unlikely at 0.1 wt% in PMMA films, since at such a low concentration the molecules are well-isolated from each other. On the other hand, when different spectra are recorded over time, this means that the total luminescence comes from different states (e.g. triplet states) at different times.

The analysis of the spectra acquired for **X1**, **X4** and **X7** in PMMA after different time delays (Fig. 6) shows that different phenomena are occurring depending on time delay and temperature. In all cases, there is a high-energy emission at RT and early times (450 nm, 2.3–10 ns) that is weak for **X1** and **X7** (Fig. 6b and d) and more intense for **X4** (Fig. S11, ESI†). This emission is attributed to a locally excited state ^{1}LE from direct excitation and emission from the D or A moiety. At longer times, the initial weak ^{1}LE emission disappears, and after TD = 0.5 µs to 2 µs only the CT emission remains. At this stage, the band onset remains the same, even when the time delay increases by several orders of magnitude (TD **X1** = 200 µs, TD **X4** = 250 µs, TD **X7** = 500 µs). This is taken as an indication of TADF emission for these molecules in PMMA at RT. Additional confirmation comes from the decay profiles (Fig. 6c, e and Fig. S11c, ESI†) that extend to 1 ms with an average lifetime of 59.5 µs for **X1**, 53.0 µs for **X4**, and 56.8 µs for **X7**. Finally, we have investigated the intensity dependence of the DF emission as a function of the laser excitation dose (Fig. S13, ESI†). The 100 ns to 30 µs time span was analysed and a linear slope of 0.99 ± 0.01 was found. This result confirms a monomolecular process typical of TADF (as opposed to TTA, which is a bimolecular process). The energies of the CT singlet excited states were thus obtained from the onset of the pure CT emission (TD = 0.5–2 µs) and are estimated at ES(**X1**) = 2.70 eV, ES(**X4**) = 2.64 eV and ES(**X7**) = 2.63 eV respectively.

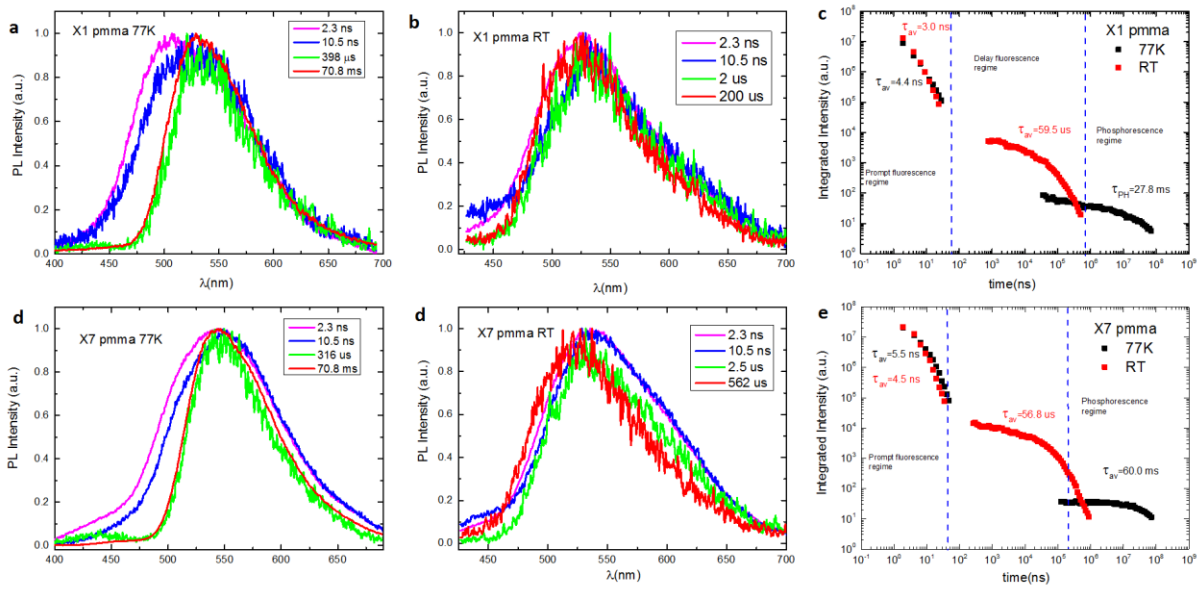

Fig. 6 Time-resolved emission spectra at increasing delay times for **X1** (a and b) and **X7** (d and e) in PMMA films, at 77 K (right) and room temperature (center). Decay curves at room temperature and 77 K for **X1** (c) and **X7** (f).

The 77 K spectra for all compounds show at early times a broad emission band that contains a mixture of LE and CT contributions (Fig. 6a, d and Fig. S11a (ESI†), TD = 2.3–10.5 ns, see also comparison of RT and 77 K spectra in Fig. S12a–c, ESI†). At later times, a narrow band is observed, whose onset is red shifted compared to the CT emission at RT. Emission decays (Fig. 6c, e and Fig. S11c, ESI†) show a contribution in the nanosecond regime typical of PF emission and a very long delayed emission in the millisecond regime characteristic of phosphorescence. Intermediate times were also studied for **X4** and it is possible to see a clear DF contribution. The origin of this low temperature DF is unclear: it could be TADF (ΔE_{ST} of **X4** is small, vide infra), or TTA, or even a mix of both phenomena.

The energies of the first triplet states were obtained from the onsets of the 77 K spectra with the longest delay, corresponding to pure phosphorescence emission. They are estimated at E_T(**X1**) = 2.58 eV, E_T(**X4**) = 2.50 eV and E_T(**X7**) = 2.52 eV. Subtracting E_T from E_S it is possible to obtain the very important ΔE_{ST} energy gap: ΔE_{ST}(**X1**) = 0.12 eV, ΔE_{ST}(**X4**) = 0.14 eV and ΔE_{ST}(**X7**) = 0.11 eV. These relatively small singlet–triplet energy gaps (less than 150 meV) explains why a long decay time typical of TADF emission is observed at RT: the available thermal energy allows the triplet to up convert back to the singlet.

A parameter describing convincingly the amount of TADF produced is the delayed/prompt fluorescence ratio (DF/PF). The calculated values (Table 3) indicate that TADF is moderately active for these compounds. This means that the rISC rate should be higher than both phosphorescence and triplet non-radiative deactivation rates (i.e. $k_{risc} > (k_{ph} + k_{nr}(T))$. The low QYs (Table 3) indicate that the non-radiative deactivation process are strong for these systems.

Table 3 Photophysical properties of **X1**, **X4** and **X7** in solid state[a]

Comp.	QY[b] (%)	λ_{PF}, (nm)	$\lambda_{Phos.}$, (nm)	DF/PF	S_1/T_1, (eV)	ΔE_{S1-T1} (eV)	$\tau_{1,av.}$ RT/77K (ns)	$\tau_{2,av}$ RT/77K (µs)	$\tau_{3,av.}$ RT/77K (ms)
X1 PMMA	1.2	523	529	2.0	2.70/2.58	0.12	3.0/4.4	59.5/-	-/27.8
X1 neat film	1.2	538, 580 (s)	580, 628(s)	-	2.53/2.24	0.29	2.3/4.8	n.m	3.2/23.6
X1 powder	0.4	n.m.	n.m.	-	2.43/n.m	n.m	n.m	n.m	n.m
X4 PMMA	0.8	525	535	2.0	2.64/2.50	0.14	5.3/11.3	53.0/4.4	-/23.8
X4 neat film	0.4	542	581, 630 (s)	-	2.56/2.21	0.35	6.1/2.0	0.25/1.8	3.2/18.0
X4 powder	0.6	n.m.	n.m.	-	2.45/ n.m	n.m	n.m	n.m	n.m
X7 PMMA	2.0	531	546	2.7	2.63/2.52	0.11	4.5/5.5	56.8/-	-/60.0
X7 neat film	0.4	504	552, 592(s)	2.8	2.66/2.33	0.33	6.8/5.0	6.8/7.5	-/4.7
X7 powder	0.2	n.m.	n.m.	-	2.68/ n.m	n.m	n.m	n.m	n.m

[a] n.m= not measured. [b] Measured in air.

*Time-resolved photophysical properties in **X1**, **X4** and **X7** neat films* Similarly to what is observed with steady-state photoluminescence, the time-dependent PL properties of **X1**, **X4** and **X7** polycrystalline films are significantly different from PMMA films or toluene solutions. The steady-state emission spectra of those neat films are composed of several bands (vide supra). Time-resolved emission spectra and decays were collected to evaluate the origin of each peak. The emission properties of **X1**, **X4** and **X7** at different time delays are provided in Fig. 7 and Fig. S14 (ESI†) and compared in Fig. S15 (ESI†).

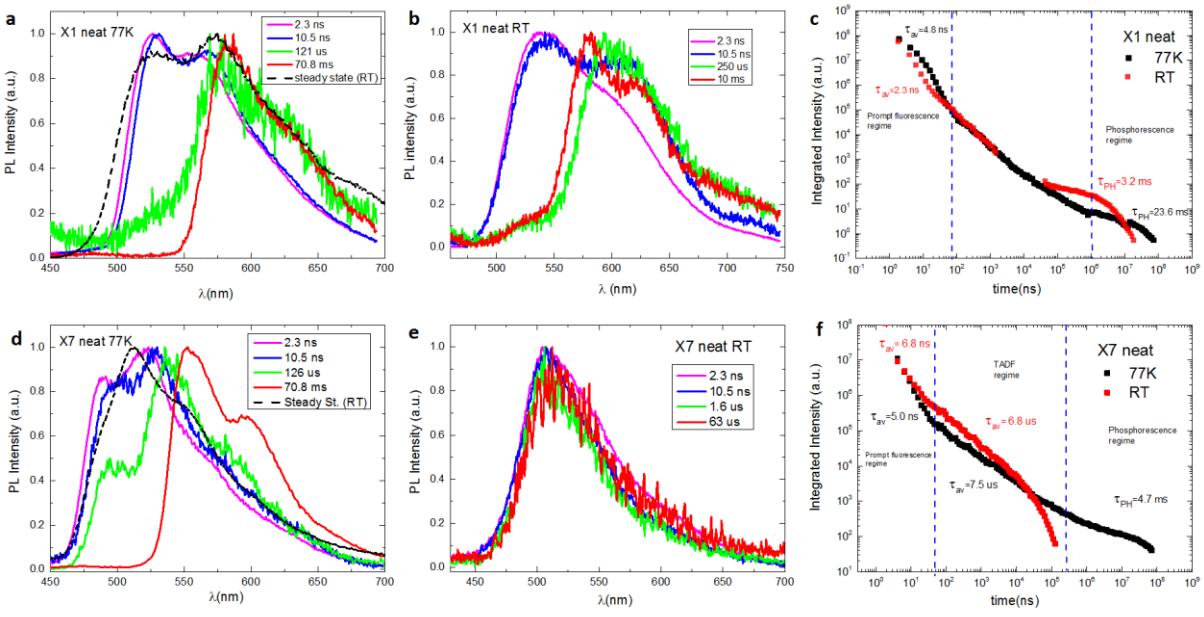

Fig. 7 Time-resolved emission spectra and decay of **X1** and **X7** in neat film: (a and d) time-resolved spectra at 77 K in comparison of the steady state (st) (b and e) time-resolved spectra at room temperature, and (c and f) decay curves at room temperature and 77 K.

For **X1** the early time (2.3 ns) emission at RT is broad with a maximum at 538 nm and a shoulder at 580 nm (Fig. 7b). However, at 77 K two resolved bands are observed at 526 nm and 560 nm (Fig. 7a). Nevertheless, the onset is quite similar (E_{onset}(RT) = 2.53 eV; E_{onset}(77 K) = 2.50 eV). At 77 K, the blue-shifted and more resolved emission is due to the rigidochromic effect, which reduces the degrees of freedom of molecular vibrational relaxation. At intermediate times, a red-shifted band appears in the spectra at both RT and 77 K, located at 594 nm and 583 nm respectively. The blue band becomes a shoulder centred at ~530 nm after 50 μs at RT and 70 μs at 77 K. This shoulder extends up to the microsecond regime at RT, which indicates the presence of a very weak DF contribution. Finally, at long delay times up to 10 ms, the RT spectra appear sharpen and peaks at 580 nm showing vibronic structure, which can be ascribed to phosphorescence. However, at 77 K the blue shoulder disappears and only the phosphorescence remains. This indicates that the blue shoulder is singlet emission from TTA (far more accessible in neat films compared to in dilute PMMA), and the red band is triplet emission. Compared to the emission of **X1** in PMMA, the blue band matches well with the CT emission. The red band observed at RT at intermediate times is observed neither at low temperature nor in the dilute PMMA films: therefore, we assume it must be a thermally activated excimer state. This can form only at RT probably because the molecules have more freedom to undergo some degree of geometry reorganization in S_1 that favours the excimer formation.

Two characteristic averaged decay times have been extracted from the decay kinetics at RT and 77 K; (Fig. 7c): a short one at 2.3 ns (and 4.8 ns at 77 K) and a long one at 3.2 ms (and 23.6 ms at 77 K). The blue band at ≈530 nm is predominant at short times at both temperatures. It is thus attributed to the prompt fluorescence of **X1**. More interestingly, the red band at 580–600 nm is attributed to a long-lived phosphorescence emission that could be observed at 77 K and RT. The comparison of the steady-state emission and time-resolved spectra (Fig. 7a and Fig. S16a, ESI†) shows that the structure observed in the former comes from the two time-resolved bands in the latter, thus demonstrating that RTP is present in neat films and even in aerated conditions (for steady-state measurements).

X4 behaves similarly to **X1** (Fig. S14, ESI†). At early times (2.3 ns) the spectra at 77 K comprises three resolved bands at 515 nm, 532 nm and 549 nm and a shoulder at 595 nm (Fig. S14a, ESI†) and the RT emission is broad with a maximum at 542 nm (Fig. S14b, ESI†). The onset of the RT early time emission is blue shifted by 0.1 eV compared to 77 K (Fig. S14c (ESI†), E_{onset}(RT) = 2.64 eV; E_{onset}(77 K) = 2.55 eV). At longer times, after 550 μs and 4 ms for RT and 77 K respectively, emission maxima and onset are strongly red shifted and the early emission band completely disappears. These characteristics indicate again the presence of phosphorescence emission both at RT and 77 K. Three characteristic times have been extracted from the decay curves in the nanosecond, microsecond and millisecond regimes at RT (and 77 K; Fig. S14d, ESI†): a short one at 6.1 ns (2.0 ns at 77 K), an intermediate one at 0.25 μs (1.8 μs) and a long one at 3.2 ms (18.0 ms). The short time is typical of PF. Conversely, the long one is attributed to the phosphorescence emission and the intermediate one to DF. TADF is unlikely because of the large singlet–triplet energy gap (ΔE_{ST} = 0.35 eV, Table 3) and therefore the DF emission is ascribed to TTA. This large ΔE_{ST} gap also promotes RTP by preserving a large triplet population with low rISC rate.[61,62] The clearly red shifted emission at 77 K after a delay time of 17 μs is probably due to a mix between TTA and phosphorescence. Finally, at long delay times (after 550 μs and 4 ms for 77 K and RT respectively) a red-shifted band appears in the spectra located at 594 nm at RT and 581 nm at 77 K. As for **X1**, the red band at 580–600 nm is attributed to a long-lived phosphorescence emission that could be observed at 77 K and RT.

X7, despite its structural similarity to **X1**, exhibits a markedly different behaviour, resembling more **X4** (Fig. 7). Its early time (2.3 ns) emission at RT is narrower than either **X1** or **X4**, with a maximum at 504 nm (Fig. 7b), this does not change over 60 μs and is clearly similar to the CT emission compared to the PMMA spectra. However, at 77 K two resolved bands are observed at 491 nm and 523 nm and a shoulder at 570 nm (Fig. 7a). The onset for both early time measurements is

quite similar (E_{onset}(RT) = 2.66 eV; E_{onset}(77 K) = 2.67 eV). This indicates that at RT a new species dominates the radiative decay compared to 77 K. Tentatively we ascribe this to thermally activated rotation about the D–A dihedral bond stabilising the CT state at RT but hindered at 77 K leaving structured local emission followed by phosphorescence at long times. This all points to flattening of the molecules in the crystal form that requires large amounts of thermal energy to force twisting of the D–A to yield a stable CT state. At long delay times, comparison of the time-resolved emission spectra at RT and 77 K (Fig. S16c, ESI†) reveals that the **X7** neat film does not show RTP. In fact, while at 77 K clear phosphorescence is observed with a millisecond delay time, the same does not happen at RT where the emission ends before reaching 100 μs, indicative of thermally activated non-radiative decay.

These two observations demonstrate that **X7** polycrystalline neat films emit entirely from the same state as the single molecule, without forming emissive aggregates and maintaining DF properties. The origin of this DF is once again unclear: it could be TADF, or TTA, or even a mix of both phenomena. We suggest that the lack of RTP for this material is due to a different packing environment of the **X7** crystal, differing significantly from **X1** and **X4**. Indeed, the 3,6-di-*tert*-butylcarbazole is more hindered than the unsubstituted carbazole in **X1** and **X4**. This makes **X7** molecules lie more distant from each other and they are less likely to form intermolecular π–π stacking which allow to avoid both aggregated (dimer or excimer) emissive states and ACQ in neat films or when packed in the crystal. Several examples are reported in literature[56,58,63–65] where bulky substituents are used to avoid aggregation quenching phenomena, while carbazole containing materials have been shown to form persistent dimer states.[56,66] This explain why **X7** maintains the photophysical characteristics of the single molecule with only DF emission in the polycrystalline film.

Comparison of phosphorescence emission in PMMA and neat film The shape, onset and phosphorescence maxima of **X1**, **X4** and **X7** in neat films (Fig. 5) are very different from doped PMMA films (Fig. 5). For all compounds, the emission in PMMA is Gaussian, while the emission in neat film is structured with vibronic features typical of phosphorescence (Fig. 5 and Fig. S17, ESI†). In PMMA, both the phosphorescence maxima (λ_{PH}(**X1**) = 529 nm, λ_{PH}(**X4**) = 535 nm and λ_{PH}(**X7**) = 546 nm) and especially the phosphorescence onset (E_T(**X1**) = 2.58 eV, E_T(**X4**) = 2.50 eV and E_T(**X7**) = 2.52 eV) are similar for all the three compounds, thus indicating that emission probably arises from the same triplet state. Since carbazole has a triplet energy at 3.20 eV, we can exclude this groups as responsible for the phosphorescence of **X1**, **X4** and **X7**. Therefore, we suggest that it arises from the ^{3}LE of the as-triazine acceptor. On the other hand the phosphorescence of neat films looks similar for **X1** (λ_{PH}(**X1**) = 580 nm, 628(s) nm; E_{onset}(**X1**) = 2.24 eV) and **X4** (λ_{PH}(**X4**) = 581 nm, 630(s) nm; E_{onset}(**X4**) = 2.21 eV) and is strongly red-shifted compared to PMMA films (Fig. S17a and b, ESI†). This indicates that the origin of the phosphorescence emission in **X1** and **X4** neat films is different from PMMA. We suggest that in neat films the phosphorescence arises from the formation of a low-lying triplet aggregated state, which is favoured by the close proximity of the molecules in the solid state. This interpretation is also corroborated by the work of Zhongfu An et al.[66,67] In particular, they reported three different carbazolyl-1,3,5-triazine derivatives which present a strong phosphorescence very similar to that of our compounds. In their publication, they indicate that the phosphorescence arises from the formation of H-aggregates. The formation of aggregates is hindered by *tert*-butyl groups in **X7**, thus maintaining single-molecule-like emission. This is clearly indicated by the similar onset of the PF time resolved and steady state spectra in PMMA and neat film for **X7** alone.

*Comparison between the photophysical properties of **X1**, **X4** and **X7** in PMMA and neat films* Table 3 summarizes the spectroscopic data for **X1**, **X4** and **X7** in solid state, to provide a comparative screening of their emission properties. We have seen so far that **X1** and **X4** show RTP. This is possible because in a solid rigid medium, and in particular in crystals (close proximity and ordered array), large-amplitude motions, collision with solvent molecules and diffusion of oxygen molecules that occurs in solution (each of which provide efficient paths for non-radiative deactivation) are suppressed. In organic molecules, in general, the transition between the triplet and the singlet

ground state is spin-forbidden, and so the triplet state's radiative decay rate ($k_r(T)$) is considerably longer than the singlet state radiative ($k_r(S)$) and all non-radiative (k_{nr}) ones. However, in our molecules, the radiative decay rate from the triplet state becomes able to compete with non-radiative decay processes that are considerably slowed down, even at room temperature, enabling RTP to be observed. Furthermore, intersystem crossing that populates the lowest triplet excited state is favored in this class of materials by the presence of n–π* electronic transitions.[68–71]

Finally, as we have shown above, both **X1** and **X4** exhibit RTP in neat films, contrarily to PMMA films where they present only TADF at RT, and phosphorescence at 77 K. In contrast, **X7** presents TADF both in neat films and PMMA at RT, and phosphorescence only at 77 K. DFT calculations show that at the S_0 geometry, ΔE_{ST} is large, because all three compounds have a rather flat structure with a partially delocalized HOMO. On the other hand, at the S_1 (CT) geometry, the compounds are more twisted and ΔE_{ST} is small. Therefore, we suggest that in PMMA, which is a soft polymer, it is possible for the compounds to undergo partial reorganization in the excited state so that ΔE_{ST} decreases, leading to TADF at RT and phosphorescence at 77 K (a temperature where the polymer is much stiffer). However, in neat films, in addition to the formation of poly crystalline order, **X1** and **X4** are more constrained, so the reorganization is not possible and a large ΔE_{ST} is maintained even after excitation to S_1. This means that TTA becomes favoured at the expense of slow TADF, and the appearance of RTP at longer times. In the case of **X7** the bulky *tert*-butyl substituents reduced intermolecular packing and so the molecules may be able to undergo some level of reorganization, while at 77 K the frozen environment blocks all molecular motions, leading to the observed phosphorescence.

What we thus observe for **X7** is a competition between TADF/TTA in the early DF region which depletes the triplet population leaving only weak phosphorescence at later times. As TTA is frozen out at lower temperatures then more intense phosphorescence is observed (further assisted by reduced non-radiative decay). Thus, in these Cz derivatives we are observing a complex interplay between the competition of TTA/TADF, non-radiative decay and phosphorescence. The different effects of temperature on all these processes gives rise to the various photophysical properties of each compound. In PMMA where TTA is ruled out through high intermolecular separation at the low concentrations used, we see a simpler competition between non-radiative decay and phosphorescence. In this case very slow TADF can be observed, as confirmed by the linear excitation power dependencies found.

Conclusions

A series of seven new D–A compounds featuring a benzofuro[3,2-*e*]-1,2,4-triazine or a benzothieno[3,2-*e*]-1,2,4-triazine moiety as the electron acceptor and carbazole, phenothiazine or phenoxazines has been synthesized. The derivatives **X2**, **X3**, **X5** and **X6** comprising an azine (phenothiazine, phenoxazine) as a donor are only weakly emissive, likely because of the existence of a large distortion between the two subunits. On the other hand, the compounds featuring a carbazole donor display interesting photophysical properties. TADF is observed when the molecules are in solution or immobilized in a PMMA matrix, i.e. in the isolate state. In drop cast microcrystalline neat films we instead observe DF in a complex competition between TTA and TADF. This outcompetes any slow TADF and sets up a complex competition between TTA, non-radiative decay and phosphorescence, which are highly temperature and material dependent. A full study demonstrates that the carbazole containing **X1** and **X4** present crystallization induced phosphorescence emission at room temperature in neat films indicative of greatly reduced non radiative decay channels, while **X7**, which comprises a bulky 3,6-di-*tert*-butylcarbazole, displays only singlet DF, indicating the strong effect these side groups have on molecular packing and photophysical properties. The new acceptor introduced in this work can thus induce very different and complex photophysical properties in solution and solid state with only subtle changes in their

structure, which greatly affects the competition between different photophysical decay mechanisms. This subunit and strategy for control of photophysical properties will likely enable the development of new efficient emissive materials in future.

Conflicts of interest

There are no conflicts to declare.

Acknowledgements

The research leading to these results has received funding from the European Union's Horizon 2020 research and innovation programme under the Marie Skłodowska-Curie grant agreement number 674990 (EXCILIGHT) and 732013 (HyperOLED).

Notes and references

1. A. Endo , M. Ogasawara , A. Takahashi , D. Yokoyama , Y. Kato and C. Adachi , Thermally activated delayed fluorescence from Sn(4+)-porphyrin complexes and their application to organic light emitting diodes--a novel mechanism for electroluminescence, Adv. Mater., 2009, 21 , 4802 —4806.
2. T. Nakagawa , S. Y. Ku , K. T. Wong and C. Adachi , Electroluminescence based on thermally activated delayed fluorescence generated by a spirobifluorene donor-acceptor structure, Chem. Commun., 2012, 48 , 9580 —9582.
3. S. Y. Lee , T. Yasuda , H. Nomura and C. Adachi , High-efficiency organic light-emitting diodes utilizing thermally activated delayed fluorescence from triazine-based donor-acceptor hybrid molecules, Appl. Phys. Lett., 2012, 101 , 093306.
4. J. Lee , K. Shizu , H. Tanaka , H. Nomura , T. Yasuda and C. Adachi , Oxadiazole- and triazole-based highly-efficient thermally activated delayed fluorescence emitters for organic light-emitting diodes, J. Mater. Chem. C, 2013, 1 , 4599 —4604.
5. H. Tanaka , K. Shizu , H. Nakanotani and C. Adachi , Twisted Intramolecular Charge Transfer State for Long-Wavelength Thermally Activated Delayed Fluorescence, Chem. Mater., 2013, 25 , 3766 —3771.
6. X. Zhen , R. Qu , W. Z. Chen , W. Wu and X. Q. Jiang , The development of phosphorescent probes for in vitro and in vivo bioimaging, Biomater. Sci., 2021, 9 , 285 —300.
7. Y. S. Wang , H. Q. Gao , J. Yang , M. M. Fang , D. Ding , B. Z. Tang and Z. Li , High Performance of Simple Organic Phosphorescence Host-Guest Materials and their Application in Time-Resolved Bioimaging, Adv. Mater., 2021, 33 , 2007811.
8. Q. Zhang , H. Kuwabara , W. J. Potscavage Jr. , S. Huang , Y. Hatae , T. Shibata and C. Adachi , Anthraquinone-based intramolecular charge-transfer compounds: computational molecular design, thermally activated delayed fluorescence, and highly efficient red electroluminescence, J. Am. Chem. Soc., 2014, 136 , 18070 —18081.
9. X. Han , Q. Bai , L. Yao , H. C. Liu , Y. Gao , J. Y. Li , L. Q. Liu , Y. L. Liu , X. X. Li , P. Lu and B. Yang , Highly Efficient Solid-State Near-Infrared Emitting Material Based on Triphenylamine and Diphenylfumaronitrile with an EQE of 2.58% in Nondoped Organic Light-Emitting Diode, Adv. Funct. Mater., 2015, 25 , 7521 —7529.
10. E. Hontz , W. D. Chang , D. N. Congreve , V. Bulovic , M. A. Baldo and T. Van Voorhis , The Role of Electron-Hole Separation in Thermally Activated Delayed Fluorescence in Donor-Acceptor Blends, J. Phys. Chem. C, 2015, 119 , 25591 —25597.
11. Y. Tao , K. Yuan , T. Chen , P. Xu , H. H. Li , R. F. Chen , C. Zheng , L. Zhang and W. Huang , Thermally Activated Delayed Fluorescence Materials Towards the Breakthrough of Organoelectronics, Adv. Mater., 2014, 26 , 7931 —7958.
12. F. B. Dias , T. J. Penfold and A. P. Monkman , Photophysics of thermally activated delayed fluorescence molecules, Methods Appl. Fluoresc., 2017, 5 , 012001.
13. Y. Im , M. Kim , Y. J. Cho , J. A. Seo , K. S. Yook and J. Y. Lee , Molecular Design Strategy of Organic Thermally Activated Delayed Fluorescence Emitters, Chem. Mater., 2017, 29 , 1946 —1963.

14. Z. Y. Yang , Z. Mao , Z. L. Xie , Y. Zhang , S. W. Liu , J. Zhao , J. R. Xu , Z. G. Chi and M. P. Aldred , Recent advances in organic thermally activated delayed fluorescence materials, Chem. Soc. Rev., 2017, 46 , 915 —1016.
15. M. Y. Wong and E. Zysman-Colman , Purely Organic Thermally Activated Delayed Fluorescence Materials for Organic Light-Emitting Diodes, Adv. Mater., 2017, 29 , 1605444.
16. X. Liang , Z. L. Tu and Y. X. Zheng , Thermally Activated Delayed Fluorescence Materials: Towards Realization of High Efficiency through Strategic Small Molecular Design, Chem. – Eur. J., 2019, 25 , 5623 —5642.
17. R. S. Nobuyasu , J. S. Ward , J. Gibson , B. A. Laidlaw , Z. J. Ren , P. Data , A. S. Batsanov , T. J. Penfold , M. R. Bryce and F. B. Dias , The influence of molecular geometry on the efficiency of thermally activated delayed fluorescence, J. Mater. Chem. C, 2019, 7 , 6672 —6684.
18. P. Stachelek , J. S. Ward , P. L. dos Santos , A. Danos , M. Colella , N. Haase , S. J. Raynes , A. S. Batsanov , M. R. Bryce and A. P. Monkman , Molecular Design Strategies for Color Tuning of Blue TADF Emitters, ACS Appl. Mater. Interfaces, 2019, 11 , 27125 —27133.
19. J. S. Ward , A. Danos , P. Stachelek , M. A. Fox , A. S. Batsanov , A. P. Monkman and M. R. Bryce , Exploiting trifluoromethyl substituents for tuning orbital character of singlet and triplet states to increase the rate of thermally activated delayed fluorescence, Mater. Chem. Front., 2020, 4 , 3602 —3615.
20. Y. H. Lee , D. Lee , T. Lee , J. Lee , J. Jung , S. Yoo and M. H. Lee , Impact of boryl acceptors in para-acridine-appended triarylboron emitters on blue thermally activated delayed fluorescence OLEDs, Dyes Pigm., 2021, 188 , 109224.
21. N. A. Kukhta , H. F. Higginbotham , T. Matulaitis , A. Danos , A. N. Bismillah , N. Haase , M. K. Etherington , D. S. Yufit , P. R. McGonigal , J. V. Grazulevicius and A. P. Monkman , Revealing resonance effects and intramolecular dipole interactions in the positional isomers of benzonitrile-core thermally activated delayed fluorescence materials, J. Mater. Chem. C, 2019, 7 , 9184 —9194.
22. G. Haykir , M. Aydemir , A. Danos , S. Gumus , G. Hizal , A. P. Monkman and F. Turksoy , Effects of asymmetric acceptor and donor positioning in deep blue pyridyl-sulfonyl based TADF emitters, Dyes Pigm., 2021, 194 , 109579.
23. A. Danos , D. Gudeika , N. A. Kukhta , R. Lygaitis , M. Colella , H. F. Higginbotham , A. N. Bismillah , P. R. McGonigal , J. V. Grazulevicius and A. P. Monkman , Not the sum of their parts: understanding multi-donor interactions in symmetric and asymmetric TADF emitters, J. Mater. Chem. C, 2022, 10 , 4737 —4747.
24. Y. Kondo , K. Yoshiura , S. Kitera , H. Nishi , S. Oda , H. Gotoh , Y. Sasada , M. Yanai and T. Hatakeyama , Narrowband deep-blue organic light-emitting diode featuring an organoboron-based emitter, Nat. Photonics, 2019, 13 , 678.
25. T. Hatakeyama , K. Shiren , K. Nakajima , S. Nomura , S. Nakatsuka , K. Kinoshita , J. P. Ni , Y. Ono and T. Ikuta , Ultrapure Blue Thermally Activated Delayed Fluorescence Molecules: Efficient HOMO-LUMO Separation by the Multiple Resonance Effect, Adv. Mater., 2016, 28 , 2777 —2781.
26. A. Pershin , D. Hall , V. Lemaur , J.-C. Sancho-Garcia , L. Muccioli , E. Zysman-Colman , D. Beljonne and Y. Olivier , Highly emissive excitons with reduced exchange energy in thermally activated delayed fluorescent molecules, Nat. Commun., 2019, 10 , 597.
27. G. Y. Meng , L. J. Liu , Z. C. He , D. Hall , X. Wang , T. Peng , X. D. Yin , P. K. Chen , D. Beljonne , Y. Olivier , E. Zysman-Colman , N. Wang and S. N. Wang , Multi-resonant thermally activated delayed fluorescence emitters based on tetracoordinate boron-containing PAHs: colour tuning based on the nature of chelates, Chem. Sci., 2022, 13 , 1665 —1674.
28. D. Hall , S. M. Suresh , P. L. dos Santos , E. Duda , S. Bagnich , A. Pershin , P. Rajamalli , D. B. Cordes , A. M. Z. Slawin , D. Beljonne , A. Kohler , I. D. W. Samuel , Y. Olivier and E. Zysman-Colman , Improving Processability and Efficiency of Resonant TADF Emitters: A Design Strategy, Adv. Opt. Mater., 2020, 8 , 1901627.
29. M. Hempe , N. A. Kukhta , A. Danos , M. A. Fox , A. S. Batsanov , A. P. Monkman and M. R. Bryce , Vibrational Damping Reveals Vibronic Coupling in Thermally Activated Delayed Fluorescence Materials, Chem. Mater., 2021, 33 , 3066 —3080.
30. M. Hayduk , S. Riebe and J. Voskuhl , Phosphorescence Through Hindered Motion of Pure Organic Emitters, Chem. – Eur. J., 2018, 24 , 12221 —12230.
31. G. Giacomelli , A. Porcheddu and L. De Luca , 1,3,5 -triazine: A versatile heterocycle in current applications of organic chemistry, Curr. Org. Chem., 2004, 8 , 1497 —1519.
32. P. Audebert , G. Clavier and C. Allain , Progress, Heterocyclic Chemistry, 2017, 29.
33. P. Audebert and C. Allain , Progress in Heterocyclic Chemistry, 2018, 30.
34. G. W. Gribble , J. A. Joule , A. M. Prokhorov and D. N. Kozhevnikov , Progress in Heterocyclic Chemistry, 2011, 23.

35. T. N. Lewis , C. Tonnele , W. G. Shuler , Z. A. Kasun , H. Sato , A. J. Berges , J. R. Rodriguez , M. J. Krische , D. Casanova and C. J. Bardeen , Chemical Tuning of Exciton versus Charge-Transfer Excited States in Conformationally Restricted Arylene Cages, J. Am. Chem. Soc., 2021, 143 , 18548 —18558.
36. J. Luo , J. Z. Lu and J. Zhang , Carbazole-triazine based donor-acceptor porous organic frameworks for efficient visible-light photocatalytic aerobic oxidation reactions, J. Mater. Chem. A, 2018, 6 , 15154 —15161.
37. A. E. Nikolaenko , M. Cass , F. Bourcet , D. Mohamad and M. Roberts , Thermally Activated Delayed Fluorescence in Polymers: A New Route toward Highly Efficient Solution Processable OLEDs, Adv. Mater., 2015, 27 , 7236 —7240.
38. R. Braveenth and K. Y. Chai , Triazine-Acceptor-Based Green Thermally Activated Delayed Fluorescence Materials for Organic Light-Emitting Diodes, Materials, 2019, 12 , 2646.
39. A. Huang , Z. H. Yin , X. X. Ban , W. Jiang , Y. Dai , J. Y. Zhang , Y. Y. Liu , Y. P. Yang and Y. M. Sun , Thermally activated delayed fluorescence of N-phenylcarbazole and triphenylamine functionalised tris(aryl)triazines, Dyes Pigm., 2015, 117 , 141 —148.
40. Y. Lee , S. J. Woo , J. J. Kim and J. I. Hong , Blue thermally activated delayed fluorescence emitter using modulated triazines as electron acceptors, Dyes Pigm., 2020, 172 , 107864.
41. H. Kaji , H. Suzuki , T. Fukushima , K. Shizu , K. Suzuki , S. Kubo , T. Komino , H. Oiwa , F. Suzuki , A. Wakamiya , Y. Murata and C. Adachi , Purely organic electroluminescent material realizing 100% conversion from electricity to light, Nat. Commun., 2015, 6 , 8476.
42. Y. P. Xiang , S. L. Gong , Y. B. Zhao , X. J. Yin , J. J. Luo , K. L. Wu , Z. H. Lu and C. L. Yang , Asymmetric-triazine-cored triads as thermally activated delayed fluorescence emitters for high-efficiency yellow OLEDs with slow efficiency roll-off, J. Mater. Chem. C, 2016, 4 , 9998 —10004.
43. H. Neunhoeffer Comprehensive Heterocyclic Chemistry , A. R. Katritzky and C. W. Rees, 1984.
44. G. Seitz and J. Richter , Donor-Substituted Benzonitriles As Side-Chain Dienophiles In The Intramolecular 4 + 2 Cyclo-Addition With Inverse Electron Demand, Chem. Ber., 1989, 122 , 2177 —2181.
45. L. Salah , M. K. Etherington , A. Shuaib , A. Danos , A. A. Nazeer , B. Ghazal , A. Prlj , A. T. Turley , A. Mallick , P. R. McGonigal , B. F. E. Curchod , A. P. Monkman and S. Makhseed , Suppressing dimer formation by increasing conformational freedom in multi-carbazole thermally activated delayed fluorescence emitters, J. Mater. Chem. C, 2021, 9 , 189 —198.
46. A. Stockmann , J. Kurzawa , N. Fritz , N. Acar , S. Schneider , J. Daub , R. Engl and T. Clark , Conformational control of photoinduced charge separation within phenothiazine-pyrene dyads, J. Phys. Chem. A, 2002, 106 , 7958 —7970.
47. V. M. Vydia , S. Pola and P. Chetti , Optoelectronic and charge transport properties of D-n-A type 1,3,5-triazine derivatives: A combined experimental and DFT study, Spectrochim. Acta, Part A, 2021, 245 , 118940.
48. J. S. Brinen and L. Goodman , Low-resolution analysis of n- pi (3000 a) absorption spectrum of s-triazine, J. Chem. Phys., 1961, 35 , 1219 —1225.
49. P. L. Santos , J. S. Ward , P. Data , A. S. Batsanov , M. R. Bryce , F. B. Dias and A. P. Monkman , Engineering the singlet-triplet energy splitting in a TADF molecule, J. Mater. Chem. C, 2016, 4 , 3815 —3824.
50. J. A. Vanallan , R. E. Adel and G. A. Reynolds , Polynuclear heterocycles. 1. 1H-Benzo b pyridol 1,2,3-mn phenoxazin-1-1 and related substances, J. Org. Chem., 1962, 27 , 1659 —1664.
51. A. Courcot , D. N. Tran , B. Fraisse , F. Bonhomme , A. Marsura and N. E. Ghermani , Electronic properties of 3,3'-dimethyl-5,5'-bis(1,2,4-triazine): Towards design of supramolecular arrangements of N-heterocyclic Cu-I complexes, Chem. – Eur. J., 2007, 13 , 3414 —3423.
52. N. Mataga , Y. Torihashi and K. Ezumi , Electronic structures of carbazole and indole and the solvent effects on the electronic spectra, Theor. Chim. Acta, 1964, 2 , 158 —167.
53. M. H. Tsai , T. H. Ke , H. W. Lin , C. C. Wu , S. F. Chiu , F. C. Fang , Y. L. Liao , K. T. Wong , Y. H. Chen and C. I. Wu , Triphenylsilyl- and Trityl-Substituted Carbazole-Based Host Materials for Blue Electrophosphorescence, ACS Appl. Mater. Interfaces, 2009, 1 , 567 —574.
54. P. Pander , A. Swist , R. Turczyn , S. Pouget , D. Djurado , A. Lazauskas , R. Pashazadeh , J. V. Grazulevicius , R. Motyka , A. Klimash , P. J. Skabara , P. Data , J. Soloducho and F. B. Dias , Observation of Dual Room Temperature Fluorescence-Phosphorescence in Air, in the Crystal Form of a Thianthrene Derivative, J. Phys. Chem. C, 2018, 122 , 24958 —24966.
55. A. Reichardt Solvatochromic dyes as solvent polarity indicators, Chem. Rev., 1994, 94 , 2319 —2358.
56. M. K. Etherington , N. A. Kukhta , H. F. Higginbotham , A. Danos , A. N. Bismillah , D. R. Graves , P. R. McGonigal , N. Haase , A. Morherr , A. S. Batsanov , C. Pflumm , V. Bhalla , M. R. Bryce and A. P. Monkman , Persistent Dimer Emission in Thermally Activated Delayed Fluorescence Materials, J. Phys. Chem. C, 2019, 123 , 11109 —11117.

57. A. Cho , M. K. Hong , V. Coropceanu and J. L. Bredas , The Role of Intermolecular Interactions on the Performance of Organic Thermally Activated Delayed Fluorescence (TADF) Materials, Adv. Opt. Mater., 2021, 9 , 2002135.
58. H. Langhals , R. Ismael and O. Yuruk , Persistent fluorescence of perylene dyes by steric inhibition of aggregation, Tetrahedron, 2000, 56 , 5435 —5441.
59. M. K. Etherington Thermally Activated Delayed Fluorescence: Beyond the Single Molecule, Front. Chem., 2020, 8 , 716.
60. P. Pander , P. Data and F. B. Dias , Time-resolved Photophysical Characterization of Triplet-harvesting Organic Compounds at an Oxygen-free Environment Using an iCCD Camera, J. Visualized Exp., 2018, 142 , e56614.
61. R. J. Huang , J. Avo , T. Northey , E. Chaning-Pearce , P. L. dos Santos , J. S. Ward , P. Data , M. K. Etherington, M. A. Fox , T. J. Penfold , M. N. Berberan-Santos , J. C. Lima , M. R. Bryce and F. B. Dias , The contributions of molecular vibrations and higher triplet levels to the intersystem crossing mechanism in metal-free organic emitters, J. Mater. Chem. C, 2017, 5 , 6269 —6280.
62. A. B. Dias , K. N. Bourdakos , V. Jankus , K. C. Moss , K. T. Kamtekar , V. Bhalla , J. Santos , M. R. Bryce and A. P. Monkman , Triplet Harvesting with 100% Efficiency by Way of Thermally Activated Delayed Fluorescence in Charge Transfer OLED Emitters, Adv. Mater., 2013, 25 , 3707 —3714.
63. S. P. Anthony Organic Solid-State Fluorescence: Strategies for Generating Switchable and Tunable Fluorescent Materials, ChemPlusChem, 2012, 77 , 518 —531.
64. Y. Kubota , J. Uehara , K. Funabiki , M. Ebihara and M. Matsui , Strategy for the increasing the solid-state fluorescence intensity of pyrromethene-BF2 complexes, Tetrahedron Lett., 2010, 51 , 6195 —6198.
65. A. M. Xie , Z. D. An , M. Xie , Y. Q. Li , G. H. Zhang , S. J. Zou , L. Chen , J. D. Chen , T. Cheng and J. X. Tang , tert-Butyl substituted hetero-donor TADF compounds for efficient solution-processed non-doped blue OLEDs, J. Mater. Chem. C, 2020, 8 , 5769 —5776.
66. Z. An , C. Zheng , Y. Tao , R. Chen , H. Shi , T. Chen , Z. Wang , H. Li , R. Deng , X. Liu and W. Huang , Stabilizing triplet excited states for ultralong organic phosphorescence, Nat. Mater., 2015, 14 , 685 —690.
67. Z. K. He , C. Q. Ke and B. Z. Tang , Journey of Aggregation-Induced Emission Research, ACS Omega, 2018, 3 , 3267 —3277.
68. M. Hussain , J. Z. Zhao , W. B. Yang , F. F. Zhong , A. Karatay , H. G. Yaglioglu , E. A. Yildiz and M. Hayvali , Intersystem crossing and triplet excited state properties of thionated naphthalenediimide derivatives, J. Lumin., 2017, 192 , 211 —217.
69. W. J. Zhao , Z. K. He , J. W. Y. Lam , Q. Peng , H. L. Ma , Z. G. Shuai , G. X. Bai , J. H. Hao and B. Z. Tang , Rational Molecular Design for Achieving Persistent and Efficient Pure Organic Room-Temperature Phosphorescence, Chem, 2016, 1 , 592 —602.
70. C. Kenry and B. Liu , Enhancing the performance of pure organic room-temperature phosphorescent luminophores, Nat. Commun., 2019, 10 , 2111.
71. Z. He , W. Zhao , J. W. Y. Lam , Q. Peng , H. Ma , G. Liang , Z. Shuai and B. Z. Tang , White light emission from a single organic molecule with dual phosphorescence at room temperature, Nat. Commun., 2017, 8 , 416.